# Capabilities and incapabilities of unity power factor control algorithm for DSTATCOM under abnormal grid and load conditions

Yogesh Rohilla*

EEE Department,
Institute of Engineering and Technology,
JK Lakshmipat University,
Jaipur, India
Email: yogeshrohilla1@gmail.com
*Corresponding author

Dinesh Kumar

Global R&D Center,
Department of EMC and Harmonics,
Danfoss Drives A/S,
Grasten 6300, Denmark
Email: dinesh@danfoss.com

Bharat Singh Rajpurohit

School of Computing and Electrical Engineering,
Indian Institute of Technology (IIT) Mandi,
Himachal Pradesh, India
Email: bsr@iitmandi.ac.in

**Abstract:** Distribution static compensator (DSTATCOM) is an efficient custom power device to enhance the power quality of distribution network. To operate the DSTATCOM, a control strategy is a must and the unity power factor (UPF) is one such control strategy, which is used in DSTATCOM applications. The UPF algorithm has been developed in such a way that it operates as the reference supply current generator for DSTATCOM. To ensure the effective operation of DSTATCOM, it is important to analyse the performance of selected control algorithm at different disturbances either coming from source side or load side. A three-phase four-wire distribution system is considered for this study and the performance of UPF-based DSTATCOM system has been analysed for different disturbances such as unbalanced and harmonic distortion coming from source and load side. Exhaustive analysis is provided using the simulation tools (MATLAB/Simulink) to show the capabilities and incapabilities of UPF control algorithm under such disturbances. Each case is analysed thoroughly keeping the view of reactive power requirement, load balancing, total harmonic distortion levels as per IEEE-519 standard and power factor improvement.

**Keywords:** current distortion; distribution static compensator; DSTATCOM; unbalancing; unity power factor; UPF; control algorithm; voltage distortion.

**Reference** to this paper should be made as follows: Rohilla, Y., Kumar, D. and Rajpurohit, B.S. (2022) 'Capabilities and incapabilities of unity power factor control algorithm for DSTATCOM under abnormal grid and load conditions', *Int. J. Power Electronics*, Vol. 15, No. 1, pp.55–85.

**Biographical notes:** Yogesh Rohilla received his Master of Technology (Gold Medallist) in Power Systems from the National Institute of Technology Kurukshetra, Haryana, India, in 2011. He served in the Sharda Group of Institution, Agra-Mathura, India from 2011–2013 and Jind Institute of Engineering and Technology, Jind, India from 2008–2009. He is currently associated with the Institute of Engineering and Technology, JK Lakshmipat University, Jaipur, India, as an Assistant Professor in Department of Electrical and Electronics Engineering. His research interests include power quality, power electronics and electric vehicles. He is a member of the Institute of Electrical and Electronics Engineers (IEEE), Institute of Research Engineers and Doctors (IRED), International Society for Research and Development (ISRD) and an associate member of International Academy of Science and Engineering for Development (IASED). He has been part of various technical program committees and reviewer of IEEE conferences and other journals.

Dinesh Kumar received his Master of Technology in Power System Engineering from the Indian Institute of Technology (IIT), Roorkee, India, in 2004 and PhD in Power Electronics from University of Nottingham, UK, in 2010. From 2004–2005, he served as a Lecturer in the Electrical Engineering Department at National Institute of Technology, Kurukshetra, India. In 2006, he joined the Technical University Chemnitz, Germany as a Research Fellow. From 2006 to 2010, he investigated and developed matrix converter-based multidrive system for aerospace applications. Since 2011, he has been with the Danfoss Drives A/S, Denmark, where he is involved in many research and industrial projects. His current research interests include motor drive, harmonic analysis and mitigation techniques, power quality and electromagnetic interference in power electronics. He is an editor of the *International Journal of Power Electronics* and associate editor of *IEEE Transaction on Industry Applications*.

Bharat Singh Rajpurohit received his MTech in Power Apparatus and Electric Drives from the Indian Institute of Technology Roorkee, Roorkee, India, in 2005 and PhD in Electrical Engineering from Indian Institute of Technology Kanpur, Kanpur, India, in 2010. He is currently an Associate Professor with the School of Computing and Electrical Engineering, Indian Institute of Technology Mandi, Mandi, India. His major research interests include electric drives, renewable energy integration and power electronics application to power systems. He is a member of the International Society for Technology in Education, Institution of Engineers (India) and Institution of Electronics and Telecommunication Engineers.

## 1 Introduction

Use of power electronic converters (PECs) is continuously growing in domestic, commercial and industrial applications to provide operating flexibility and energy efficiency (Bose, 2009). Therefore, these are very common and present in most of the applications. These power electronic-based loads are nonlinear in nature and therefore possess some disadvantages such as reactive power requirement and generation of harmonics which lead to poor power factor (PF). Moreover, these current harmonics together with grid impedance results voltage harmonic distortion at the point of common coupling (PCC) (Kumar and Zare, 2016; Zare and Kumar, 2016; Zare et al., 2017). Modern distribution network faces a variety of power quality issues such as voltage unbalance, background harmonic distortion, voltage sag, swell and so on. Recent power quality surveys show that voltage unbalance is one of major problem in modern distribution network (CEER, 2011; Brito et al., 2018; Elphick et al., 2017; Kumar et al., 2017). Root causes of voltage unbalance in a distribution network are (Von Jouanne and Banerjee, 2001):

1 unequal distribution of single-phase load on three-phase power system

2 asymmetrical feeders and transformer winding

3 asymmetrical power generation of grid connected single phase distributed generations such as roof-top solar inverters.

The use of three-phase four-wire (3P4W) configuration is common in different part of world to supply power to residential and commercial loads. The unbalance in such distribution network can overload neutral wire due to high current flow (Alam et al., 2015).

In order to improve the power quality at PCC, a number of solutions have been proposed such as passive filters, active filters, hybrid filter, etc. Passive filters are normally tuned at specific frequency. Therefore, many tuned passive filters are required in a complex system (Albatran et al., 2018; Aleem and Zobaa, 2017; Kumar and Zare, 2014; Leite et al., 2017). Moreover, passive filters have some severe drawbacks such as aging, large parameter tolerance and resonance issue with grid impedance (Das, 2003; Menti et al., 2009). Also, these passive filters will not help to improve voltage unbalancing issue. Active filters are best solution for handling many problems at a time (Akagi, 2005; Litrán et al., 2005; Rohilla and Pal, 2013; Singh et al., 1999) but their cost is relatively higher than passive filters, which eliminates them to use in many cost-sensitive applications. To minimise this drawback, various hybrid filters topologies have been reported in recent years (Asiminoaei et al., 2006; Chen and von Jouanne, 2001; George and Mishra, 2010; Gupta et al., 2011; Rahmani et al., 2009). Hybrid filters are combination of active and passive filters and could provide a cost-effective solution.

The distribution static compensator (DSTATCOM) is an example of shunt connected active filter and has the functions of reactive power compensation and harmonic mitigation. Single line diagram of DSTATCOM is shown in Figure 1. The DSTATCOM for 3P4W distribution system can be formed using different configurations such as three-leg voltage source converter (VSC) with single DC capacitor, three-leg VSC with neutral clamped DC capacitors, three-leg VSC with transformer, four-leg VSC, etc. (Iyer et al., 2005; Kumar et al., 2008; Mahela and Shaik, 2015; Srikanthan and Mishra, 2009).

The main purpose of DSTATCOM is to supply reactive power demanded by load, so that source only supply active power and results in unity power factor (UPF). If load is nonlinear in nature, then the load current ($I_L$) has both active and reactive power components. Active power requirement of load current is fulfilled by $I_S$ (source current) and reactive power requirement is fulfilled by $I_C$ (compensator current) as shown in Figure 1.

**Figure 1** Single line diagram of DSTATCOM (see online version for colours)

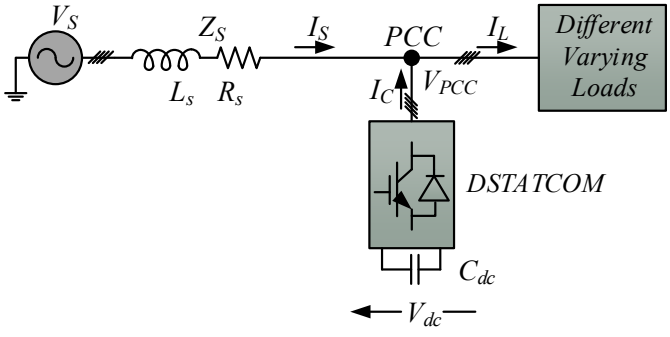


Many control algorithms are available to enable DSTATCOM to serve as a reactive power compensator at PCC (Bangarraju et al., 2014; Benysek and Pasko, 2012; Elhaj et al., 2018; Han et al., 2010; Krismanto et al., 2012; Meral and Çelik, 2018; Saralaya and Sharma, 2018). The UPF is one such algorithm (Abellan et al., 2002; Garg et al., 2014; Orts-Grau et al., 2008). Orts-Grau et al. (2008) analysed UPF control algorithm for 3P4W system. Garg et al. (2014) shows the UPF control theory performance for the induction motor fed from single-phase supply and Abellan et al. (2002) used this control algorithm for three-phase supply system. These papers analysed the UPF performance in the presence of load side disturbances. Impact of source/grid side disturbances is still unknown for this control algorithm which needs to be explored to have complete performance study. In order to fill this gap, this paper analysed the performance of UPF-based DSTATCOM control algorithm in detail and observed its capabilities and incapabilities at different grid and load profiles.

The rest of this paper is organised as follows. In Section 2, the UPF control algorithm is described analytically. In Section 3, performance of UPF is analysed under different load and grid conditions and obtained simulation results are discussed in detail. Section 4 summarises the performance of UPF control algorithm. Finally, conclusion is drawn in Section 5.

## 2 UPF control algorithm

As the name suggests the UPF control algorithm is developed to provide UPF in normal or abnormal load conditions. Any system will supply UPF if it has a resistive load. In other words, system will provide UPF if its voltage space vector is in phase with current space vector. The operating principle of UPF is to see load as a resistive component at PCC. Purpose of this control algorithms is to generate reference source currents, so that source should supply only active power and rest power requirement of load is supplied by

compensator, i.e., DSTATCOM in this study. So, reference source currents are corresponding to load but in phase with source voltage. The detail block diagram for extracting reference source currents using UPF control algorithm is shown in Figure 2.

**Figure 2** Block diagram for extracting reference source currents using UPF control algorithm (see online version for colours)

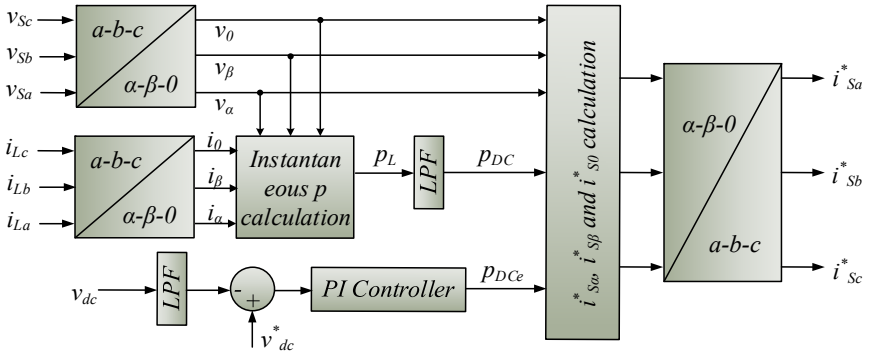


The UPF method is also known as 'voltage synchronisation method' where source current space vector is desired to be in phase with the PCC voltage space vector as shown in equation (1):

$$i_s^* = K.v \tag{1}$$

where $K$ is a constant. Value of $K$ depends on the PCC voltages ($v$) and the load. The $i_s^*$ is the required reference source currents. The power delivered by the source will be

$$p_s = v.i_s^* = K.v^2 \tag{2}$$

$v$ can be given in $\alpha$-$\beta$-$0$ plane as

$$v = \sqrt{v_0^2 + v_\alpha^2 + v_\beta^2}$$

To calculate $p_S$, load currents (i.e., $i_{La}$, $i_{Lb}$ and $i_{Lc}$) and PCC voltages (i.e., $v_{Sa}$, $v_{Sb}$ and $v_{Sc}$) are sensed and converted into $\alpha$-$\beta$-$0$ coordinates as shown in equations (3) and (4).

$$\begin{bmatrix} v_\alpha \\ v_\beta \\ v_0 \end{bmatrix} = \sqrt{\frac{2}{3}} \begin{bmatrix} 1 & -1/2 & -1/2 \\ 0 & \sqrt{3}/2 & -\sqrt{3}/2 \\ 1/\sqrt{2} & 1/\sqrt{2} & 1/\sqrt{2} \end{bmatrix} . \begin{bmatrix} v_{Sa} \\ v_{Sb} \\ v_{Sc} \end{bmatrix} \tag{3}$$

$$\begin{bmatrix} i_\alpha \\ i_\beta \\ i_0 \end{bmatrix} = \sqrt{\frac{2}{3}} \begin{bmatrix} 1 & -1/2 & -1/2 \\ 0 & \sqrt{3}/2 & -\sqrt{3}/2 \\ 1/\sqrt{2} & 1/\sqrt{2} & 1/\sqrt{2} \end{bmatrix} . \begin{bmatrix} i_{La} \\ i_{Lb} \\ i_{Lc} \end{bmatrix} \tag{4}$$

The constant $K$ can be determined with the criterion that the power delivered by the source equal to the *DC* component of the instantaneous active power of the load, so that

$$K = \frac{p_{DC} + p_{DCe}}{\left(v_0^2 + v_\alpha^2 + v_\beta^2\right)_{DC}} \tag{5}$$

$p_{DC}$ and $p_{DCe}$ are explained in equations (7) and (8), respectively. The instantaneous active power in $\alpha$-$\beta$-0 coordinates are calculated as:

$$p_L = v_\alpha \cdot i_\alpha + v_\beta \cdot i_\beta + v_0 \cdot i_0 \tag{6}$$

Total instantaneous active power ($p_L$) can be decomposed into fundamental and harmonic powers as:

$$p_L = \bar{p}_L + \tilde{p}_L = p_{DC} + p_{AC} \tag{7}$$

where $p_{DC}$ represents the *DC* component which is responsible for fundamental active power and $p_{AC}$ represents harmonic power component. As source is required to supply fundamental power ($p_{DC}$) only and the other power requirement, i.e., reactive power ($p_{AC}$) must be supplied by DSTATCOM. The fundamental instantaneous active power component can be extracted from the $p_L$ by using a low pass filter (Butterworth type).

The reference source currents in $\alpha$–$\beta$–0 reference frame can be calculated as:

$$\begin{bmatrix} i_{S\alpha}^* \\ i_{S\beta}^* \\ i_{S0}^* \end{bmatrix} = \frac{1}{Ax_{(3\varphi)}} \cdot \begin{bmatrix} v_\alpha \\ v_\beta \\ v_0 \end{bmatrix} \cdot \left[ p_{DC} + p_{DCe} \right] \tag{8}$$

where $i_{S\alpha}^*, i_{S\beta}^*$ and $i_{S0}^*$ represent the reference source current signals in $\alpha$-$\beta$-0 coordinates respectively. $Ax_{(3\varphi)} = \left(v_0^2 + v_\alpha^2 + v_\beta^2\right)_{DC}$ and $p_{DCe}$ is active power required to maintain the DC bus voltage at a constant reference value $(V_{DC}^*)$. The $p_{DCe}$ is the losses of DSTATCOM. Aim of this paper is to analyse the capabilities and incapabilities of UPF control algorithm in extracting reference source currents. For doing so, there is no need to calculate $p_{DCe}$. Good PI tuned DSTATCOM follows nearly same output characteristics as generated by control algorithms (Bangarraju et al., 2014; Orts-Grau et al., 2008; Rohilla and Pal, 2013).

Reference source currents in *a-b-c* reference frame can be calculated by inverse transformation of equation (8) as:

$$\begin{bmatrix} i_{Sa}^* \\ i_{Sb}^* \\ i_{Sc}^* \end{bmatrix} = \sqrt{\frac{2}{3}} \cdot \begin{bmatrix} 1 & 0 & 1/\sqrt{2} \\ -1/2 & \sqrt{3}/2 & 1/\sqrt{2} \\ -1/2 & -\sqrt{3}/2 & 1/\sqrt{2} \end{bmatrix} \cdot \begin{bmatrix} i_{S\alpha}^* \\ i_{S\beta}^* \\ i_{S0}^* \end{bmatrix} \tag{9}$$

where $i_{S\alpha}^*$, $i_{S\beta}^*$ and $i_{Sc}^*$ are the required reference source currents for phase *a*, phase *b* and phase *c*, respectively. These extracted reference source currents $(i_{Sa}^*, i_{Sb}^*$ and $i_{Sc}^*)$ used to generate switching signals of the DSTATCOM.

Step by step flow diagram to extract reference source currents using UPF control algorithm is shown in Figure 3. First step is to measure PCC voltages and load currents.

In second step, these measured quantities are converted into $\alpha$-$\beta$-0 reference frame from *a-b-c* reference frame. In third step, instantaneous power is calculated. In next step, this calculated power is filtered to find out DC component of it. DC component of power and $\alpha$-$\beta$-0 reference voltages are used to calculate $\alpha$-$\beta$-0 values of reference source currents in next step. In last step, $\alpha$-$\beta$-0 values are converted to *a-b-c* values to obtain required reference source currents.

**Figure 3** Flow diagram of UPF control algorithm (see online version for colours)

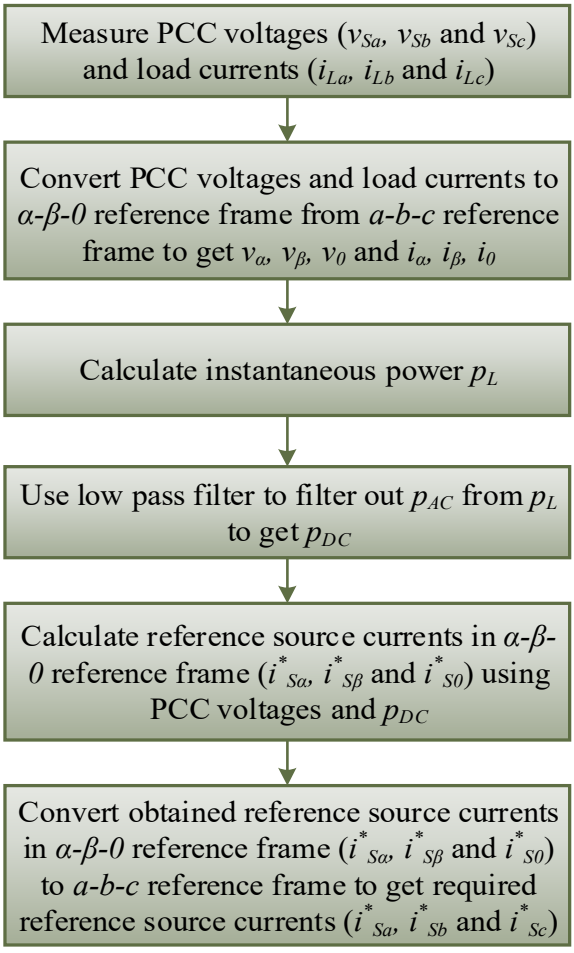


## 3 Performance evaluation of UPF control theory

In this section, performance of UPF control algorithm is analysed at different load and supply conditions as illustrated in Table 1. Simulation tool of matrix laboratory has been used for this purpose. In all the cases, a 3P4W of 415 V line-line, 50 Hz and a linear load of 20 kW with 0.8 PF has been considered in general, as shown in Figure 4. Line impedance ($Z_S$) of $(0.14 + j0.314)$ Ω has been considered for this study.

**Table 1** Different cases considered for UPF evaluation

| *Cases* | | *Source* | | *Load* | |
|---|---|---|---|---|---|
| | | *Specifications* | *Distortion* | *Specifications* | *Distortion* |
| Case I | Ideal supply voltage – balanced and undistorted load current | 415 V L-L, 50 Hz, $Z_S = (0.14 + j0.314)\ \Omega$ | No distortion | 20 kW, 0.8 PF | No distortion |
| Case II | Ideal supply voltage – balanced and distorted load current (5th, 7th, 11th harmonics) | 415 V L-L, 50 Hz, $Z_S = (0.14 + j0.314)\ \Omega$ | No distortion | 20 kW, 0.8 PF | $THD_i = 16.08\%$ |
| Case III | Distorted supply voltage (5th harmonic) – balanced and undistorted load current | 415 V L-L, 50 Hz, $Z_S = (0.14 + j0.314)\ \Omega$, 5th harmonic = 10% $V_1$ | $THD_v = 9.75\%$ | 20 kW, 0.8 PF | No distortion |
| Case IV | Distorted supply voltage (5th harmonic) – balanced and distorted load current (5th, 7th, 11th harmonics) | 415 V L-L, 50 Hz, $Z_S = (0.14 + j0.314)\ \Omega$ 5th harmonic = 10% $V_1$ | $THD_v = 9.75\%$ | 20 kW, 0.8 PF | $THD_i = 16.08\%$ |
| Case V | Ideal supply voltage – unbalanced and undistorted load current (1-phase out) | 415 V L-L, 50 Hz, $Z_S = (0.14 + j0.314)\ \Omega$ 5th harmonic = 10% $V_1$ | No distortion | 20 kW, 0.8 PF, phase 'b' out | Load unbalancing |
| Case VI | Distorted supply voltage (5th harmonic) – unbalanced and undistorted load current | 415 V L-L, 50 Hz, $Z_S = (0.14 + j0.314)\ \Omega$, 5th harmonic = 10% $V_1$ | $THD_v = 9.75\%$ | 20 kW, 0.8 PF, additional 5 Ω in phase *a* | Load unbalancing |
| Case VII | Distorted supply voltage (5th harmonic) – unbalanced and distorted load current (5th, 7th, 11th harmonics) | 415 V L-L, 50 Hz, $Z_S = (0.14 + j0.314)\ \Omega$ 5th harmonic = 10% $V_1$ | $THD_v = 9.75\%$ | 20 kW, 0.8 PF, additional 5 Ω in phase *a* | $THD_i = 16.08\%$ |
| Case VIII | Unbalanced supply voltage – balanced and undistorted load current | 415 V L-L, 50 Hz, $Z_S = (0.14 + j0.314)\ \Omega$, additional 5 Ω in phase *a* | Source unbalancing | 20 kW, 0.8 PF | No distortion |

Note: $V_1$ = Magnitude of fundamental component of source voltage.

**Figure 4** Single line diagram of system under consideration (see online version for colours)

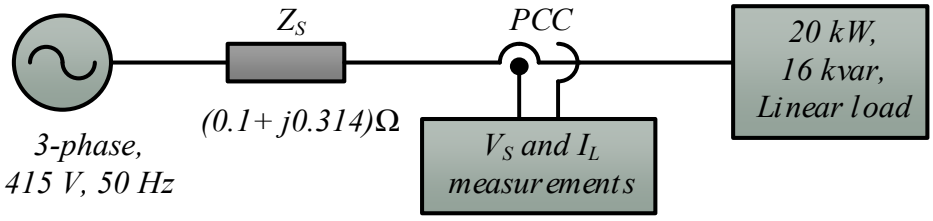


To simplify the simulation model and reduce the execution time, only linear load has been considered. While still retaining the nonlinearity in the system, harmonics are inserted in the linear loads as shown in Figure 5 (Chapman, 2001). Distortion in source, load and in reference source currents are measured by calculating total harmonic distortion (*THD*) as given in equation (10). Harmonics have been measured up to 20th order.

$$THD_x = \frac{\sqrt{x_2^2 + x_3^2 + \cdots + x_{20}^2}}{x_1} \tag{10}$$

where $x$ represents current or voltage for which distortion need to be measured. The $x_1$, $x_2$, …, $x_{20}$ are the RMS values of $x$ for 1st, 2nd, …, 20th order harmonics, respectively.

**Figure 5** Equivalent circuit of a nonlinear load (see online version for colours)

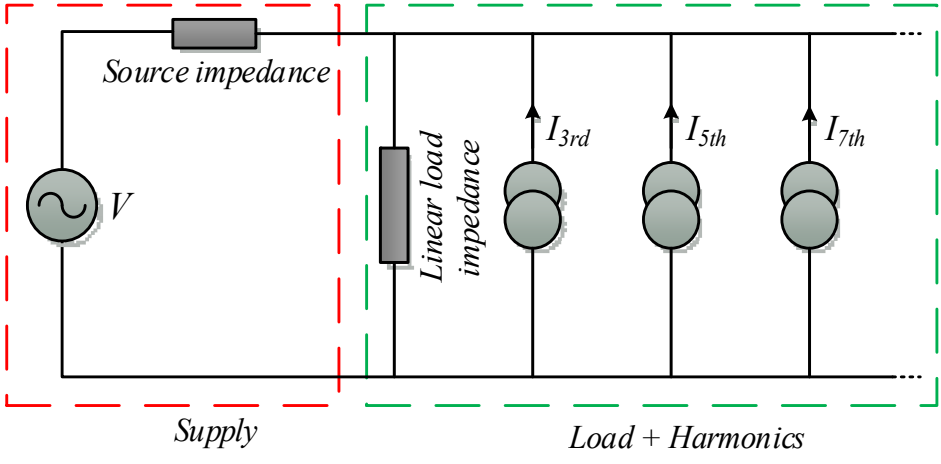


### *3.1 Case I: ideal supply voltage – balanced and undistorted load current*

For benchmarking study, balanced and undistorted grid and load conditions have been considered in this case. A 20 kW linear load is connected and PF has been kept at 0.8. Figure 6(a) shows the supply voltages ($v_S$), load currents ($i_L$) and reference supply currents ($i_S^*$). As no distortion and no unbalancing are considered, so all the three waveforms observed as sinusoidal in nature.

**Figure 6** Simulation results for Case I, (a) supply voltages, load currents, and reference source currents (b) 0-$\alpha$-$\beta$ coordinates of supply voltages (c) harmonic analysis of phase *a* of load current and reference source current (d) Source voltage and current, source voltage and reference current of phase *a* for PF analysis (see online version for colours)

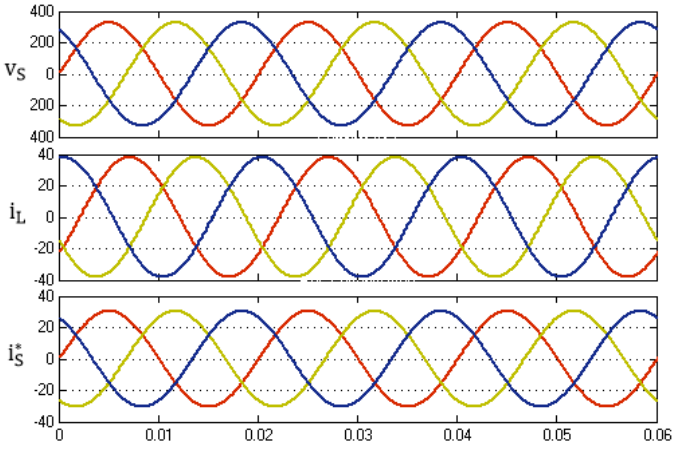


(a)

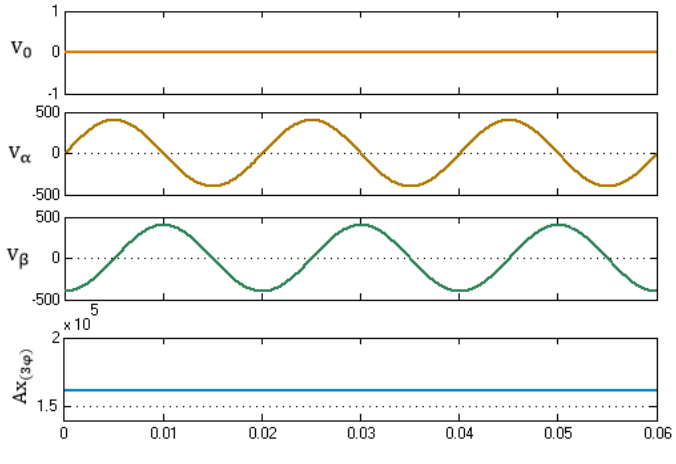


(b)

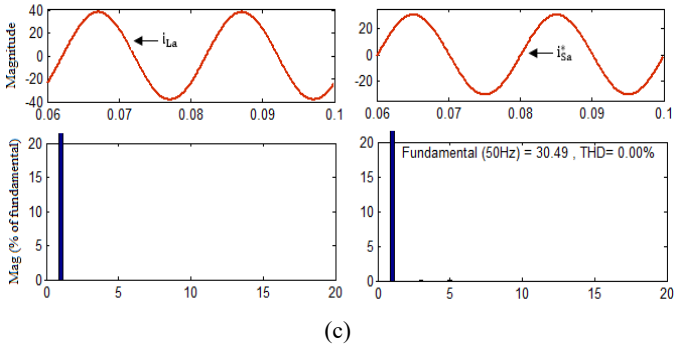


(c)

**Figure 6** Simulation results for Case I, (a) supply voltages, load currents, and reference source currents (b) 0-$\alpha$-$\beta$ coordinates of supply voltages (c) harmonic analysis of phase *a* of load current and reference source current (d) Source voltage and current, source voltage and reference current of phase *a* for PF analysis (continued) (see online version for colours)

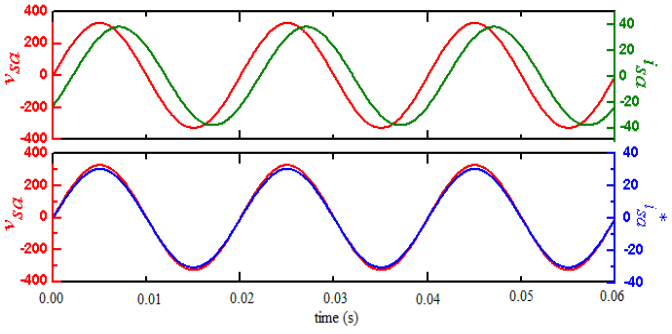


(d)

Figure 6(c) represents the harmonic analysis of load current and reference source current at PCC. Only phase *a* harmonic analysis is shown here, as harmonics are same in other two phases *b* and *c* unless system is unbalanced.

Figure 6(b) shows the four waveforms in which first three are $v_0$, $v_\alpha$ and $v_\beta$ waveforms which are 0-$\alpha$-$\beta$ reference frame converted from *a*-*b*-*c* reference frame and fourth waveform shows $Ax_{(3\varphi)}$. As observed from Figure 6(b), $v_0$ is zero and $v_\alpha$ and $v_\beta$ are 90° phase shifted.

Figure 6(d) depicts the capability of PF correction of the UPF control algorithm. In first waveform of Figure 6(d), the load has 0.8 PF lagging which can be seen from the phase difference between the waveforms of $v_{S\alpha}$ and $i_{S\alpha}$. This phase difference came down to zero as shown by $v_{S\alpha}$ and $i_{S\alpha}$, as a result, the PF has corrected to unity as shown in second waveform. Simulation results are summarised in Table 2.

**Table 2** Simulation results summary of Case I

| | $i_{La}$ | $i_{Sa}^*$ |
|---|---|---|
| $THD_i$ | 0.00 | 0.00 |
| $I$ (A) | 26.95 | 21.56 |
| $P$ (W) | 5,003 | 5,003 |
| $Q$ (var) | 3,752 | 0.038 |
| $PF$ | 0.8 | 1.0 |
| | $THD_{va}$ = 0.00 | |

In Table 2, column $i_{La}$ and column $i_{Sa}^*$ show the simulation results obtained for load current for phase *a* and reference source (grid) current for phase *a* respectively, generated by the UPF control algorithm. The $I$, $P$ and $Q$ are current, active power and reactive power respectively. In this case, the $THD$ is zero, because balanced and undistorted supply and load conditions have been considered in this case. Here, it is important to note that the $PF$ has been improved from 0.8 to 1.0, which shows the effectiveness of UPF

control algorithm. Active power ($P$) supplied by source is constant at 5,003 watts. Reactive power ($Q$) requirement of load is 3,752 vars. This reactive power is expected to supply by compensator (i.e., DSTATCOM), which is confirmed by results presented in Table 2 where UPF has successfully compensated this reactive power requirement and reduced it to 0.038 vars. Now, as the reactive power requirement has been compensated, so reference source current is reduced to 21.56 A in comparison to load requirement of 26.95 A.

'From Figure 6 and Table 2, one can conclude that UPF control theory is capable to improve PF by compensating reactive power required by load in case of ideal supply voltage, balanced and undistorted load condition.'

### *3.2 Case II: ideal supply voltage – balanced and distorted load current (5th, 7th, 11th harmonics)*

Supply voltage conditions are same as in Case I. In the load 5th, 7th and 11th harmonics are inserted (as per Figure 5) to analyse the performance of UPF control theory. Concerned waveforms are shown in Figure 7.

Figure 7(a) shows distortion in load current $i_L$ due to presence of 5th, 7th and 11th harmonics. This distortion gives 16.08% $THD_i$ in load current as shown in Figure 7(c). This distorted current passes through the source impedance, as a result source voltage gets distorted [as in Figure (a)] and around 3.04% of $THD_v$ has been recorded at PCC. Distortion in load currents has compensated by UPF at PCC and results only 3.03% $THD_i$ in source current ($i^*_{Sa}$) at PCC as shown in Figure 7(c). In Figure 7(b), $v_0$ shows the effect of distortion on 0-$\alpha$-$\beta$ reference frame whereas there is no effect on $v_\alpha$ and $v_\beta$, and both has same nature as in Case I. In Figure 7(d), effectiveness of UPF algorithm can be observed where $PF$ is improved from 0.8 to unity.

**Figure 7** Simulation results for Case II, (a) supply voltages, load currents, and reference source currents (b) 0-$\alpha$-$\beta$ coordinates of supply voltages (c) harmonic analysis of phase $a$ of load current and reference source current (d) source voltage and current, source voltage and reference current of phase $a$ for PF analysis (see online version for colours)

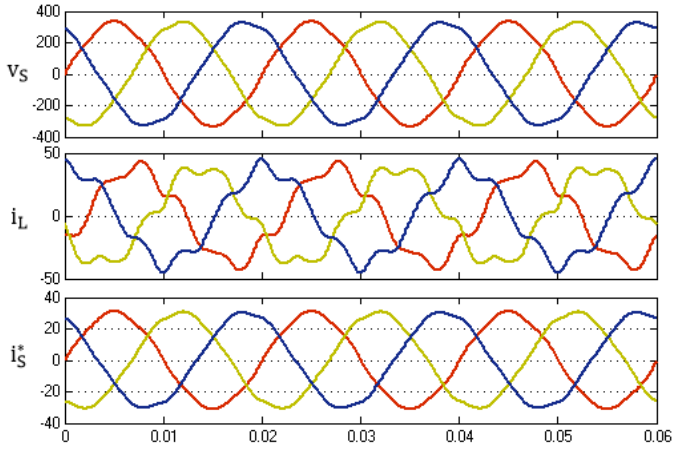


(a)

**Figure 7** Simulation results for Case II, (a) supply voltages, load currents, and reference source currents (b) 0-$\alpha$-$\beta$ coordinates of supply voltages (c) harmonic analysis of phase *a* of load current and reference source current (d) source voltage and current, source voltage and reference current of phase *a* for PF analysis (continued) (see online version for colours)

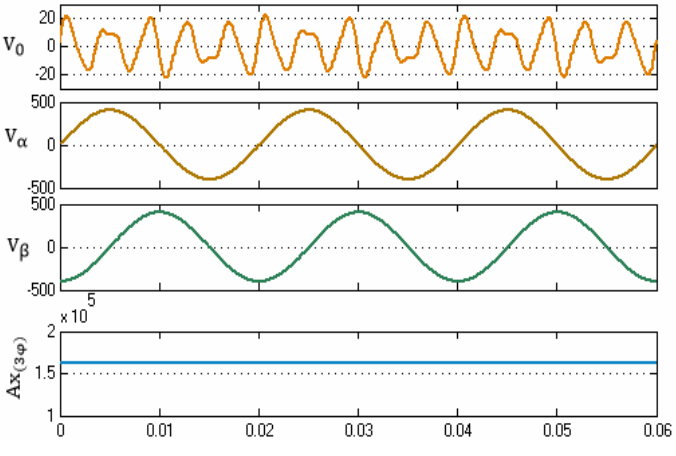


(b)

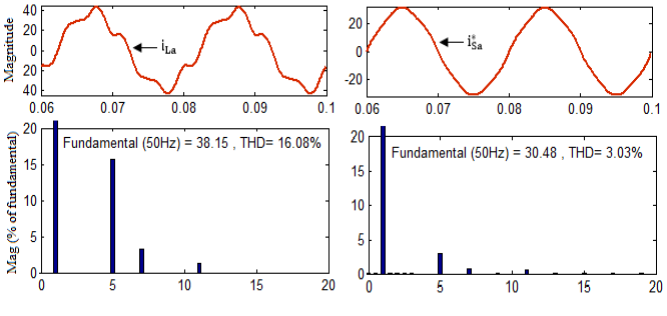


(c)

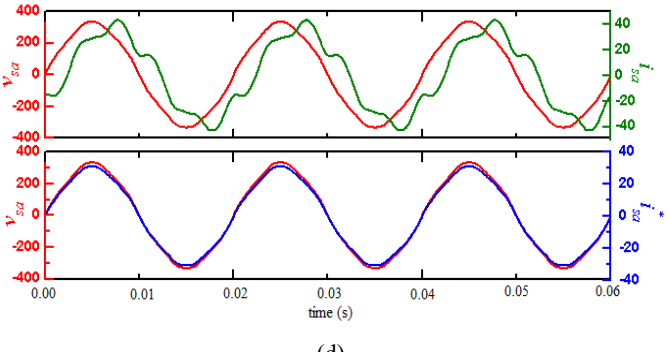


(d)

Various parameters of Case II are shown in Table 3. The UPF has maintained the UPF in this case also by compensating reactive power requirement of 3,760 vars to 0.432 vars which is nearly zero. As a result, reference source current $(i_{Sa}^{*})$ is decreased to

21.55 A in comparison to load current requirement of 26.98 A and remaining 5.43 A reactive current component supplied by DSTATCOM.

**Table 3** Simulation results summary of Case II

| | $i_{La}$ | $i^*_{Sa}$ |
|---|---|---|
| $THD_i$ | 16.08 | 3.03 |
| $I$ (A) | 26.98 | 21.55 |
| $P$ (W) | 5,013 | 5,007 |
| $Q$ (var) | 3,760 | 0.432 |
| $PF$ | 0.8 | 1.0 |
| | $THD_{va}$ = 3.04 | |

Here, it is interesting to note that compensated current and $v_{Sa}$, both are showing nearly same distortion (i.e., 3%). It seems that UPF has replicated the *THD* of source voltage in the *THD* of reference source current. This is due to fact that UPF has the property to see everything connected after PCC as resistive components but not before PCC.

'It can be concluded that UPF has compensated harmonics in load current and provided UPF at PCC.'

### *3.3 Case III: distorted supply voltage (5th harmonic) – balanced and undistorted load current*

The 5th harmonic distortion is introduced in supply voltage which results a $THD_v$ of 9.75%. Load is considered same as in Case I, i.e., balanced and undistorted. Its effect on all the other parameters is shown in Figure 8.

**Figure 8** Simulation results for Case III, (a) supply voltages, load currents, and reference source currents (b) 0-$\alpha$-$\beta$ coordinates of supply voltages (c) harmonic analysis of phase *a* of load current and reference source current (d) source voltage and current, source voltage and reference current of phase *a* for PF analysis (see online version for colours)

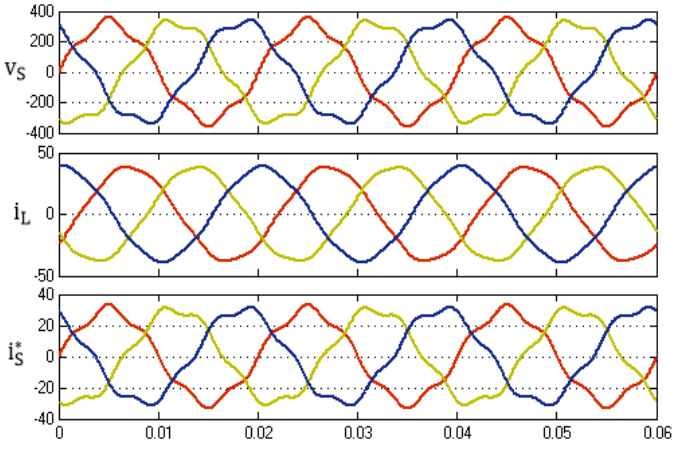


(a)

**Figure 8** Simulation results for Case III, (a) supply voltages, load currents, and reference source currents (b) 0-$\alpha$-$\beta$ coordinates of supply voltages (c) harmonic analysis of phase *a* of load current and reference source current (d) source voltage and current, source voltage and reference current of phase *a* for PF analysis (continued) (see online version for colours)

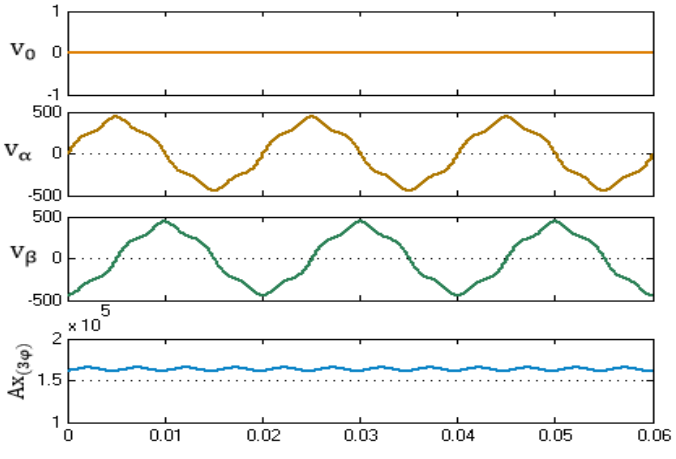


(b)

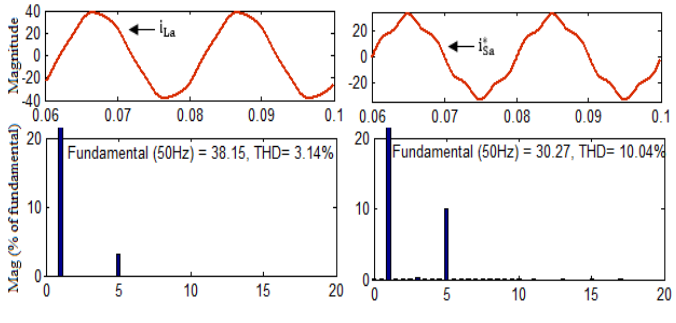


(c)

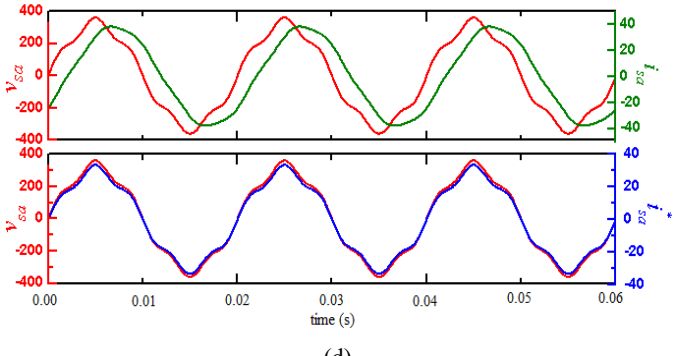


(d)

It can be seen in Figure 8(a), that $v_S$ and $i_S^*$ have same waveform pattern whereas $i_L$ has different pattern. 'It leads to the conclusion that harmonics of source is also present in reference source current.' This can also be confirmed by the data shown in Table 4.

**Table 4** Simulation results summary of Case III

| | $i_{La}$ | $i_{Sa}^{*}$ |
|---|---|---|
| $THD_i$ | 3.14 | 10.04 |
| $I$ (A) | 26.98 | 21.4 |
| $P$ (W) | 5,013 | 4,972 |
| $Q$ (var) | 3,760 | 0.078 |
| $PF$ | 0.8 | 1.0 |
| | $THD_{va} = 9.75$ | |

Voltage distortion does not affect $v_0$ but effect $v_\alpha$ and $v_\beta$, as in Figure 8(b). The $i_S^*$ has a $THD_i$ of 10.04% which is resultant of source voltage $THD_v$ plus other compensation losses. Due to distorted supply voltage, load current also shows some distortion, 3.14% as $THD_i$. 'The UPF has perfectly compensated the reactive power requirement of load and has given a UPF but has no improvement on background distortion in supply side.'

Also, from Figure 7(b) and Figure 8(b), it is observed that distortion in load shows its effect on $v_0$ but not on $v_\alpha$ and $v_\beta$ and distortion in source disturb the $v_\alpha$ and $v_\beta$ but no effect on $v_0$. Therefore, by observing the $v_0$, $v_\alpha$ and $v_\beta$ disturbances, it is possible to identify the origin of disturbance from source side or load side.

### *3.4 Case IV: distorted supply voltage (5th harmonic) – balanced and distorted load current (5th, 7th, 11th harmonics)*

In this case, both supply voltage and load current have distortion. Level of distortion is same as considered in Case II (load current $THD_i$ is 16.08%) and Case III (background supply voltage distortion $THD_v$ is 9.75%). Concerned simulation results are shown in Figure 9.

Source voltage and reference source current [Figure 9(d)] are in same phase which results UPF although both waveforms are still distorted. $v_0$ shows the same nature as was in Case II for distorted load conditions and $v_\alpha$ and $v_\beta$ show the same nature as was in Case III for distorted load conditions. Load has a $THD_i$ of 13.04% and reference source current has 12.9% as $THD_i$, replicating the voltage $THD_v$ coming from grid side. Reactive current compensation is up to the mark.

Here, one can observe that applied load current $THD_i$ was 16.08% whereas Table 5 shows 13.04% only. Similarly applied background supply voltage has $THD_v$ 9.75% but Table 5 is showing 12.62%. Reason of this change can be understood by revisiting Case II and Case III, as this case is a summation of both the above cases' distortions. Case II has a voltage $THD_v$ of 3.04% despite having no distortion in source; it is due to load harmonics interaction with source impedance as stated earlier. Similar behaviour noticed here, when applied distortion of 9.75% in voltages has increased to 12.62%. Now in Case III, load has no distortion but it showed a $THD_i$ of 3.14% due to voltage distortion. Here, it seems that this $THD_i$ has been subtracted from the load and load current $THD_i$ reduced to 13.04% from 16.08% and this is mainly due to background distortion.

**Figure 9** Simulation results for Case IV, (a) supply voltages, load currents, and reference source currents (b) 0-$\alpha$-$\beta$ coordinates of supply voltages (c) harmonic analysis of phase *a* of load current and reference source current (d) source voltage and current, source voltage and reference current of phase *a* for PF analysis (see online version for colours)

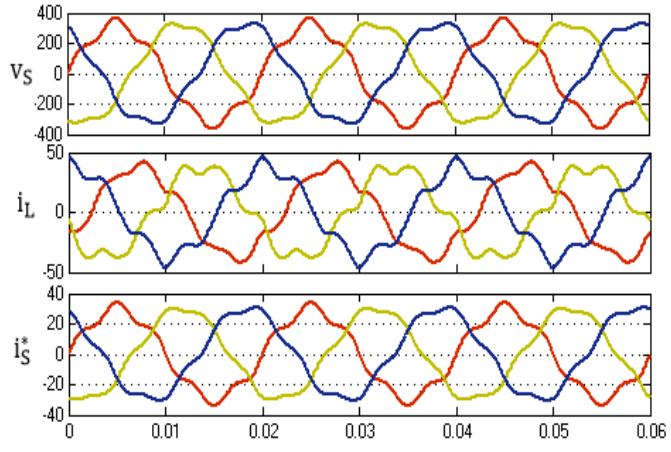


(a)

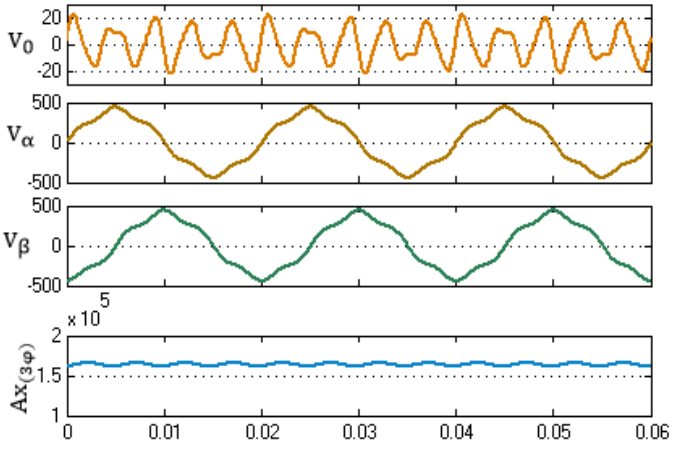


(b)

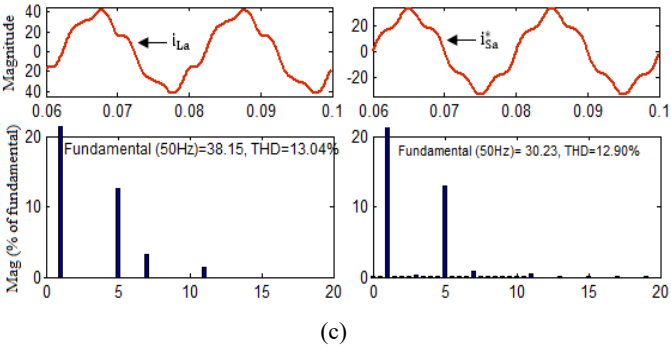


(c)

**Figure 9** Simulation results for Case IV, (a) supply voltages, load currents, and reference source currents (b) 0-$\alpha$-$\beta$ coordinates of supply voltages (c) harmonic analysis of phase *a* of load current and reference source current (d) source voltage and current, source voltage and reference current of phase *a* for PF analysis (continued) (see online version for colours)

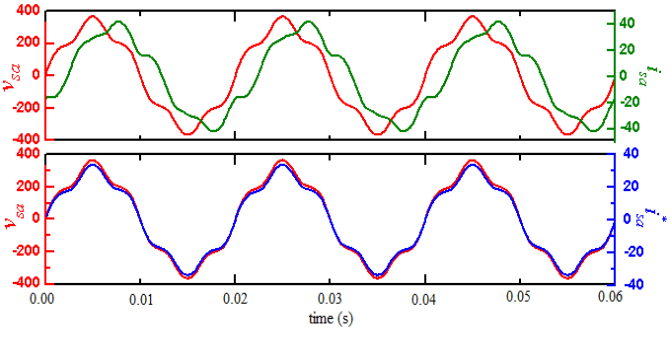


(d)

**Table 5** Simulation results summary of Case IV

| | $i_{La}$ | $i^*_{Sa}$ |
|---|---|---|
| $THD_i$ | 13.04 | 12.90 |
| $I$ (A) | 26.98 | 21.38 |
| $P$ (W) | 5,013 | 4,966 |
| $Q$ (var) | 3,760 | 0.297 |
| $PF$ | 0.8 | 1.0 |
| | $THD_{va}$ = 12.62 | |

'This shows that distortion at PCC is mainly due to background distortion (i.e., from grid side) and load side distortion has been compensated. The UPF has compensated reactive power requirement and supplied UPF in this scenario also.'

### *3.5 Case V: ideal supply voltage – unbalanced and undistorted load current (1-phase out)*

The only difference between Case I and this case is unbalancing. In this case, unbalancing in load has generated by losing of phase *b*, i.e., only two phases (phase *a* and phase *c*) have supply and third phase is open. In this case, UPF capability of balancing is on test. Figure 10 shows the concerned results.

It can be seen from Figure 10(a) that yellow phase is out. Still, algorithm managed to balance the reference current $(i^*_S)$ in three phases equally, although waveforms are not purely sinusoidal and leads to harmonic distortion with $THD_i$ of 8% in each phase.

The effects of supply unbalancing can be seen in $v_0$ waveform, as shown in Figure 10(b).

**Figure 10** Simulation results for Case V, (a) supply voltages, load currents, and reference source currents (b) 0-$\alpha$-$\beta$ coordinates of supply voltages (c) harmonic analysis of phase *a* of load current and reference source current (d) source voltage and current, source voltage and reference current of phase *a* for PF analysis (see online version for colours)

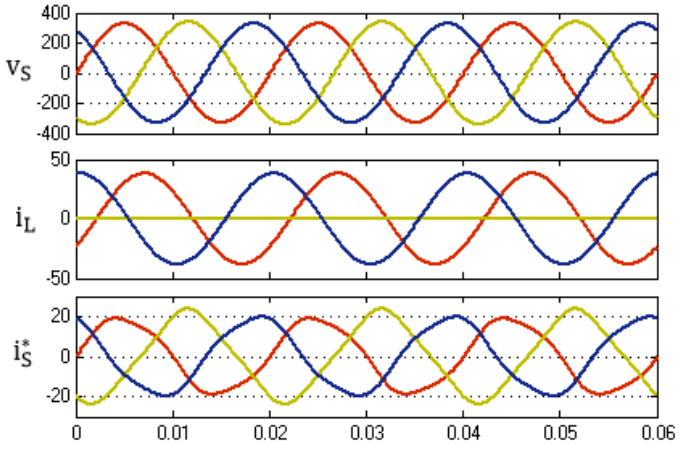


(a)

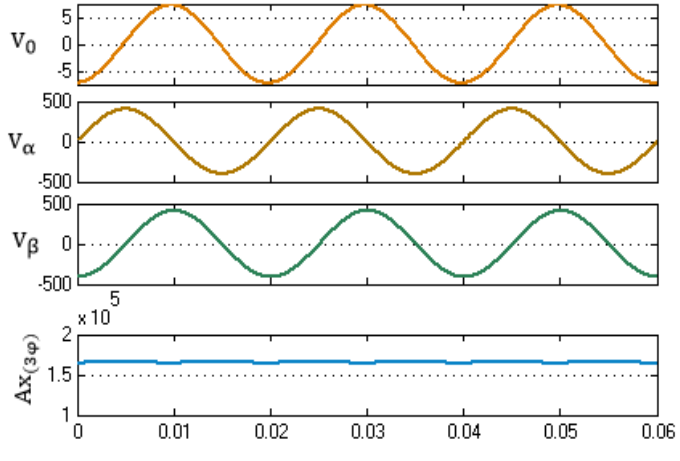


(b)

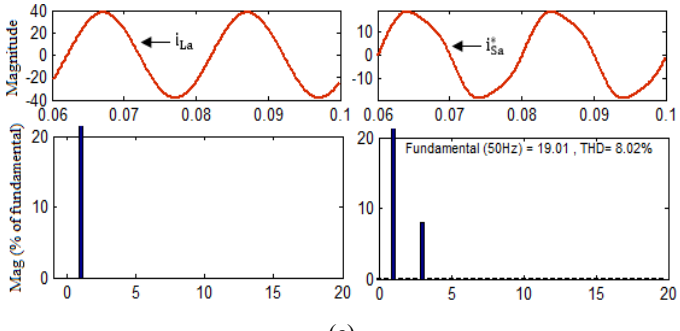


(c)

**Figure 10** Simulation results for Case V, (a) supply voltages, load currents, and reference source currents (b) 0-$\alpha$-$\beta$ coordinates of supply voltages (c) harmonic analysis of phase *a* of load current and reference source current (d) source voltage and current, source voltage and reference current of phase *a* for PF analysis (continued) (see online version for colours)

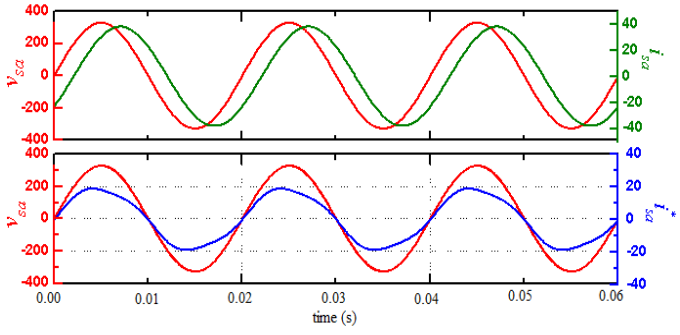


(d)

Equalisation of current in all three phases results a sharp decrease in current RMS value from 27 A to 13.44 A due to distribution of current of two healthy phases into among three phases and further due to compensation of reactive power (shown in Table 6). Negative sign of $Q$ shows reverse flow of reactive power from load to compensator. In such a critical scenario also, the UPF managed to deliver nearly UPF.

**Table 6** Simulation results summary of Case V

| | $i_{La}$ | $i^*_{Sa}$ |
|---|---|---|
| $THD_i$ | 0.00 | 8.02 |
| $I$ (A) | 26.98 | 13.44 |
| $P$ (W) | 5,013 | 3,116 |
| $Q$ (var) | 3,760 | –196.2 |
| $PF$ | 0.8 | 0.998 |
| $THD_{va} = 0.00$ | | |

'So, it is fair to say that the UPF algorithm managed to achieve UPF at PCC even under severe unbalanced load conditions.'

### *3.6 Case VI: distorted supply voltage (5th harmonic) – unbalanced and undistorted load current*

Here, 5th order harmonic is injected in supply voltage as a background distortion. Unbalance in load created by inserting 5 Ω resistance in phase *a*. Load has no harmonic distortion. Results are shown in Figure 11.

It can be observed from Figure 11(a) that due to insertion of resistance in red phase (phase *a*), current in this phase has lower magnitude than yellow (phase *b*) and blue phase (phase *c*), which show unbalanced load condition. The UPF tries to equalise the current in all the phases as seen from the waveforms of $i^*_S$ in Figure 11(a).

**Figure 11** Simulation results for Case VI, (a) supply voltages, load currents, and reference source currents (b) 0-$\alpha$-$\beta$ coordinates of supply voltages (c) harmonic analysis of phase *a* of load current and reference source current (d) source voltage and current, source voltage and reference current of phase *a* for PF analysis (see online version for colours)

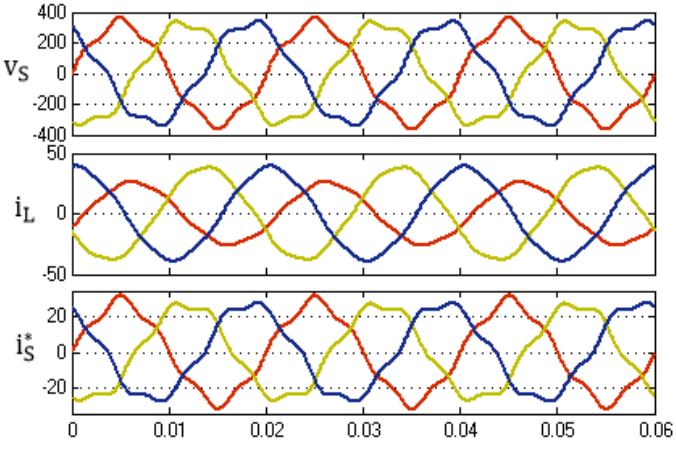


(a)

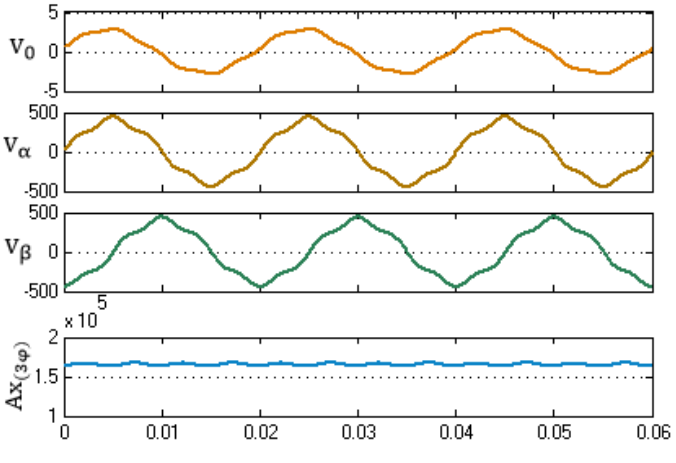


(b)

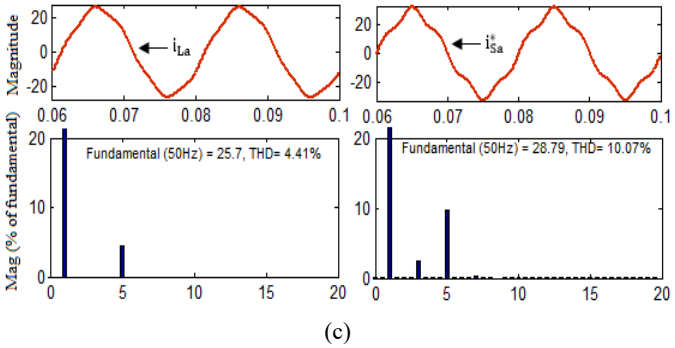


(c)

**Figure 11** Simulation results for Case VI, (a) supply voltages, load currents, and reference source currents (b) 0-$\alpha$-$\beta$ coordinates of supply voltages (c) harmonic analysis of phase *a* of load current and reference source current (d) source voltage and current, source voltage and reference current of phase *a* for PF analysis (continued) (see online version for colours)

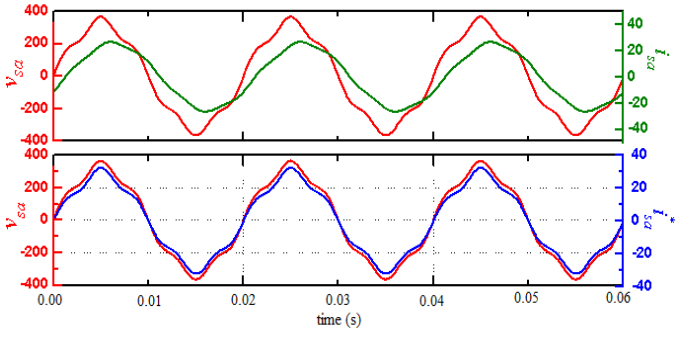


(d)

Table 7 illustrate the output parameters for the phase *a* and phase *b*. Due to presence of 5th harmonics, source voltage had a $THD_v$ of approximately 9.7% as background distortion, this results distortion in reference current ($i_S^*$) as 10.07% ($THD_i$), which is reflection of background distortion 9.7% plus some distortion due to unbalancing in load phases.

**Table 7** Simulation results summary of Case VI

| | $i_{La}$ | $i_{Sa}^*$ | $i_{Lb}$ | $i_{Sb}^*$ |
|---|---|---|---|---|
| $THD_i$ | 4.41 | 10.07 | 3.17 | 10.39 |
| $I$ (A) | 18.88 | 20.36 | 26.98 | 19.38 |
| $P$ (W) | 3,928 | 4,796 | 5,013 | 4,502 |
| $Q$ (var) | 1,707 | 27.32 | 3,760 | 66.57 |
| $PF$ | 0.917 | 1.0 | 0.8 | 0.999 |
| | $THD_{va} = 9.67$ | | $THD_{vb} = 9.75$ | |

'The UPF successfully providing UPF by compensating reactive power requirement, but no improvement has been seen in background distortion coming from grid side.'

### *3.7 Case VII: distorted supply voltage (5th harmonic) – unbalanced and distorted load current (5th, 7th, 11th harmonics)*

In this case, distortion is created in both, source and load side. Source has 5th harmonics and load has 5th, 7th and 11th harmonics. Unbalancing in load has been created as in the Case VI, i.e., by inserting 5 Ω resistors in phase *a*. Data related to phase *a* and phase *b* has been extracted and corresponding results are shown in Figure 12 and Table 8.

Due to distortion in source voltage and distorted and unbalanced load, voltage $THD_v$ for phases *a* and *b* are 12.24% and 8.21%, respectively. Table 8 shows that this voltage $THD_v$ is replicated in reference currents with some addition due to unbalance effect. The UPF has given UPF in this odd situation also. Reactive power requirement has been

compensated to very low value. The UPF tries to equalise the current in all the three phases which can be seen from Table 8, where load current in phase *a* is 18.18 A but it is compensated at source with 20.32 A and similar for phase *b* from 26.83 A at load side to 19.34 A at source side, which show how UPF controller attempt to equalise current at source side in all three phases to minimise the impact of unbalanced load condition at PCC.

'Irrespective of disturbances from source side and/or load side, the UPF achieved its target to improve PF as unity and at same time reduce load side unbalancing effects at PCC. However, again there is no improvement on background/grid side distortion.'

**Figure 12** Simulation results for Case VII, (a) supply voltages, load currents, and reference source currents (b) 0-$\alpha$-$\beta$ coordinates of supply voltages (c) harmonic analysis of phase *a* of load current and reference source current (d) source voltage and current, source voltage and reference current of phase *a* for PF analysis (see online version for colours)

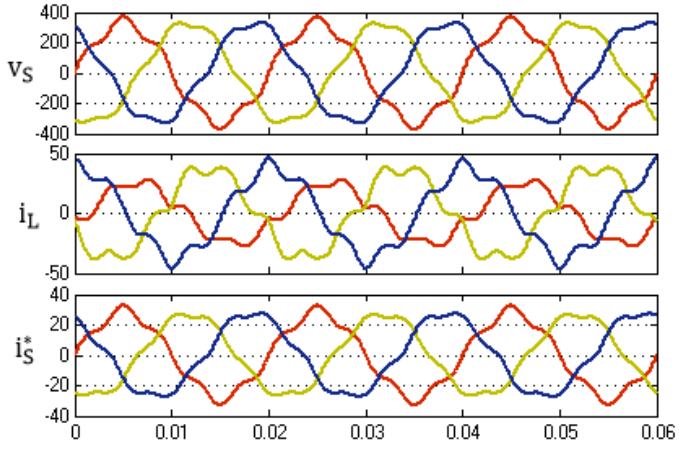


(a)

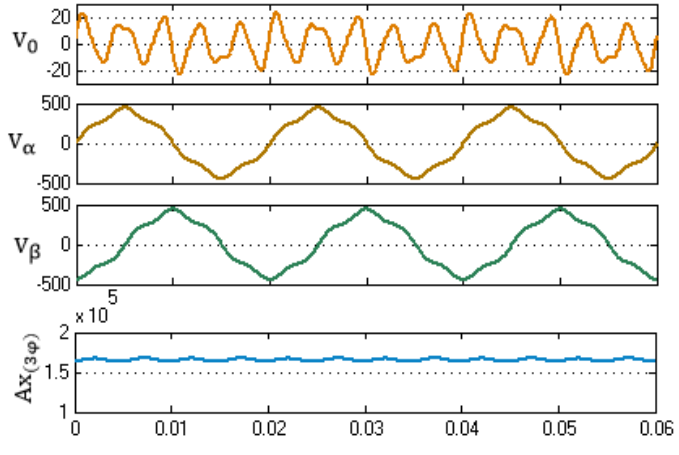


(b)

**Figure 12** Simulation results for Case VII, (a) supply voltages, load currents, and reference source currents (b) 0-$\alpha$-$\beta$ coordinates of supply voltages (c) harmonic analysis of phase *a* of load current and reference source current (d) source voltage and current, source voltage and reference current of phase *a* for PF analysis (continued) (see online version for colours)

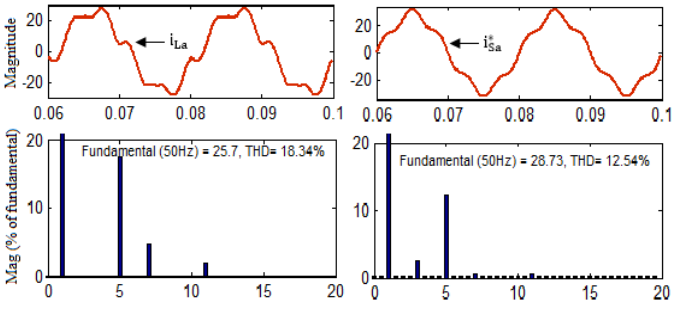


(c)

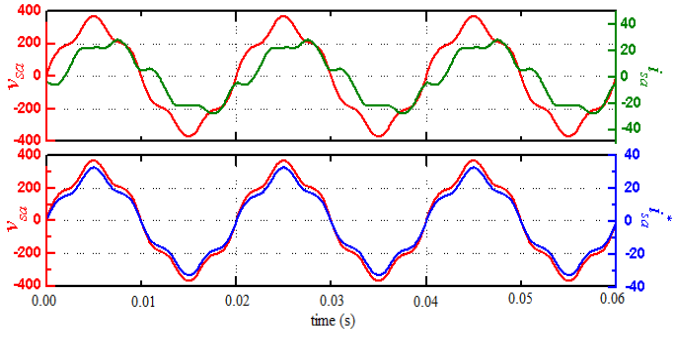


(d)

**Table 8** Simulation results summary of Case VII

| | $i_{La}$ | $i^*_{Sa}$ | $i_{Lb}$ | $i^*_{Sb}$ |
|---|---|---|---|---|
| $THD_i$ | 18.34 | 12.54 | 17.83 | 8.91 |
| $I$ (A) | 18.18 | 20.32 | 26.83 | 19.34 |
| $P$ (W) | 3,928 | 4,787 | 5,013 | 4,492 |
| $Q$ (var) | 1,707 | 28.06 | 3760 | 66.07 |
| $PF$ | 0.917 | 1.0 | 0.8 | 0.999 |
| | $THD_{va}$ = 12.24 | | $THD_{vb}$ = 8.21 | |

## *3.8 Case VIII: unbalanced supply voltage – balanced and undistorted load current*

This case shows the performance of the UPF control algorithm under unbalanced supply voltage conditions. Load is considered as balanced and without any distortion. Unbalancing in supply is created by inserting additional 5 Ω resistor (line impedance is already present) in yellow phase. Results for this case are shown in Figure 13.

**Figure 13** Simulation results for Case VIII, (a) supply voltages, load currents, and reference source currents (b) 0-$\alpha$-$\beta$ coordinates of supply voltages (c) harmonic analysis of phase *a* of load current and reference source current (d) source voltage and current, source voltage and reference current of phase *a* for PF analysis (see online version for colours)

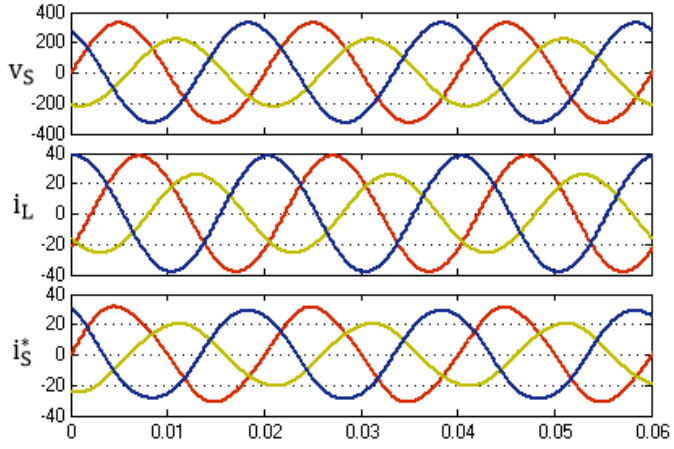


(a)

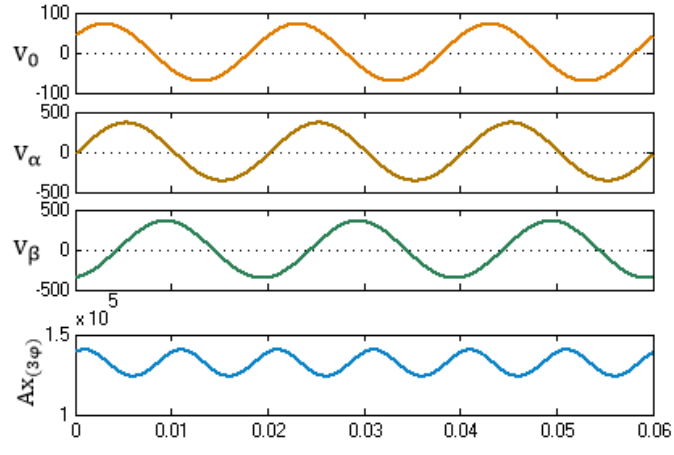


(b)

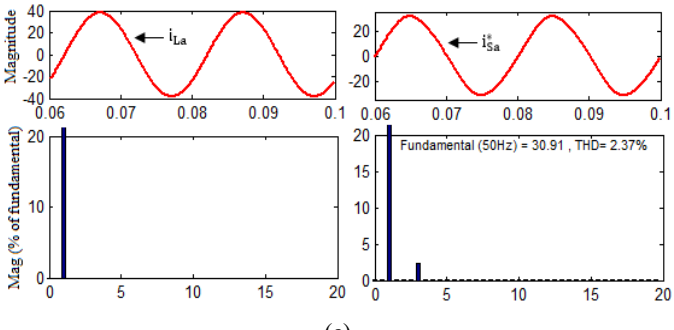


(c)

**Figure 13** Simulation results for Case VIII, (a) supply voltages, load currents, and reference source currents (b) 0-$\alpha$-$\beta$ coordinates of supply voltages (c) harmonic analysis of phase *a* of load current and reference source current (d) source voltage and current, source voltage and reference current of phase *a* for PF analysis (continued) (see online version for colours)

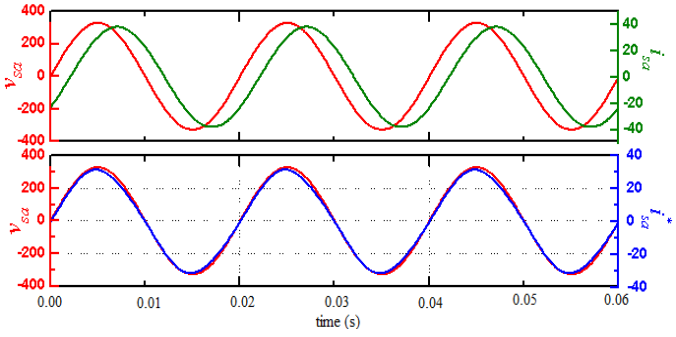


(d)

From Figure 13(a), yellow phase waveform has less magnitude than other two phases. It is due to voltage drop in 5 Ω resistor inserted in this phase. Same can be seen from the waveforms of load current and reference source current. The UPF control theory failed to balance the reference currents although it tried a little as seen from Figure 13(a). As seen in earlier cases also, 'whenever a disturbance occurs on source side, this algorithm could not observe it and fails to correct it. This fact is confirmed in this case as well.'

Unbalancing effect can be observed in $v_0$ as shown in Figure 13(b). Same can be seen from $Ax_{(3\varphi)}$ waveform. Harmonics distortion ($THD_i$) in load current is 2.37% and 2.27% in phase *a* and *b*, respectively. This distortion is result of UPF efforts to minimise the load current unbalancing effects at PCC. Although it failed, but still *PF* has been corrected perfectly to nearly unity at PCC, as shown in Figure 13(d). Other parameters are given in Table 9.

**Table 9** Simulation results summary of Case VIII

| | $i_{La}$ | $i_{S\alpha}^*$ | $i_{Lb}$ | $i_{Sb}^*$ |
|---|---|---|---|---|
| $THD_i$ | 0.00 | 2.37 | 0.00 | 2.27 |
| $I$ (A) | 26.95 | 21.85 | 18.16 | 14.51 |
| $P$ (W) | 5,003 | 5,071 | 2,271 | 2,268 |
| $Q$ (var) | 3,752 | –94.5 | 1,703 | 53.7 |
| $PF$ | 0.8 | 0.999 | 0.8 | 0.999 |
| | $THD_{va} = 0.00$ | | $THD_{vb} = 0.00$ | |

## 4 Summary

As discussed in previous section, eight cases have been considered to analyse the capabilities and incapabilities of UPF control algorithm applied for DSTATCOM under different source and load conditions. Table 10 summarise the results discussed in previous section.

**Table 10** Summary of Cases I to VIII

| *Cases* | | *Power quality before compensation* | | | | *Power quality after compensation* | | | |
|---|---|---|---|---|---|---|---|---|---|
| | | $THD_i$ *(%)* | $THD_v$ *(%)* | *PF* | *Q (var)* | $THD_i$ *(%)* | $THD_v$ *(%)* | *PF* | *Q (var)* |
| Case I | Ideal supply voltage – balanced and undistorted load current | 0 | 0 | 0.8 | 3,752 | 0 | 0 | 1 | 0.038 |
| Case II | Ideal supply voltage – balanced and distorted load current (5th, 7th, 11th harmonics) | 16.08 | 0 | 0.8 | 3,760 | 3.03 | 3.04 | 1 | 0.432 |
| Case III | Distorted supply voltage (5th harmonic) – balanced and undistorted load current | 3.14 | 9.75 | 0.8 | 3,760 | 10.04 | 9.75 | 1 | 0.078 |
| Case IV | Distorted supply voltage (5th harmonic) – balanced and distorted load current (5th, 7th, 11th harmonics) | 13.04 | 9.75 | 0.8 | 3,760 | 12.9 | 12.62 | 1 | 0.297 |
| Case V | Ideal supply voltage – unbalanced and undistorted load current (1-phase out) | 0 | 0 | 0.8 | 3,760 | 8.02 | 0 | 0.998 | –196.2 |
| | | Unbalancing in load | | | | Balanced source currents | | | |
| Case VI | Distorted supply voltage (5th harmonic) – unbalanced and undistorted load current | 3.17 | 9.75 | 0.8 | 3,760 | 10.39 | 9.75 | 0.999 | 66.57 |
| | | Unbalancing in load | | | | Balanced source currents | | | |
| Case VII | Distorted supply voltage (5th harmonic) – unbalanced and distorted load current (5th, 7th, 11th harmonics) | 17.83 | 9.75 | 0.8 | 3,760 | 8.91 | 8.21 | 0.999 | 66.07 |
| | | Unbalancing in load | | | | Balanced source currents | | | |
| Case VIII | Unbalanced supply voltage – balanced and undistorted load current | 0 | 0 | 0.8 | 1,703 | 2.27 | 0 | 0.999 | 53.7 |
| | | Unbalancing in source voltages | | | | No improvement | | | |

Table 10 provides the comparison of four power quality parameters viz. current THD ($THD_i$), voltage THD ($THD_v$), power factor ($PF$) and reactive power supplied by source ($Q$). Parameters are compared before and after implementation of selected control theory. By this comparison, capability and incapability of UPF control algorithm to tackle the issues of PF correction, harmonic reduction, reactive power compensation and unbalancing can be evaluated.

In Case I, where ideal supply voltage and balanced and undistorted load currents are taken for study, only issue was poor PF, i.e., 0.8 which required a reactive power of 3,752 var for load. After applying UPF control algorithm, $PF$ improved to unity and reactive power requirement decreased to approximately zero. In Case II, ideal supply voltage with balanced and distorted load current are considered for study. Power quality issues in this case are $THD_i$ = 16.08%, $PF$ = 0.8, $Q$ = 3,760 var. These issues can be resolved by implementing UPF algorithm, which results $THD_i$ below 5%, UPF and reactive power supplied by source reduced to 0.432 var only. Case II shows that current THD is easily handled by UPF theory and reduced to permissible limit. Case V is also related to ideal supply voltage like as Case I and Case II. In this case, unbalancing is introduced by one phase out. UPF theory has balanced these unbalanced currents and improved the PF to nearly unity. But in attempt to balancing currents, results higher $THD_i$, which is approximately 8%.

Case I and Case VIII are related to balanced and undistorted load currents, difference lies in supply voltage. Case I has balanced supply voltage and Case VIII has unbalanced supply voltage. Case I has been already discussed in previous paragraph. Output of Case VIII shows, that UPF is unable to balance the source voltages although it has improved the PF to 0.999. This unbalancing also gives rise to current distortion approximately 2.27% as $THD_i$.

Rest four cases viz. III, IV, VI and VII are related to distorted supply voltages. In these four cases, around 9.75% of $THD_v$ is created as background distortion by injecting 5th harmonic in supply voltage. UPF control theory is not able to correct the voltage distortions in these cases although it is correcting the $PF$ to unity by compensating reactive power requirement of load. This distortion in supply voltage also comes in currents as can be seen in Case III and Case VI where initially $THD_i$ were less but increased after compensation to 10.04% and 10.39% respectively.

## 5 Conclusions

In this paper, the capabilities and incapabilities of UPF control algorithm have been fully analysed at different load and grid conditions. For this purpose, eight different cases have been considered ranging from ideal conditions to highly non-ideal conditions. From all cases, it has been found that UPF control algorithm proved the worth of its name by delivering UPF even under severe non-ideal conditions both from source and load side. Providing UPF is the main goal of this control algorithm and it has been successfully verified. Also, it has been observed that UPF theory has compensated reactive power requirement of the load and therefore, source has to supply only active power, this helps to reduce nonlinearity effects of power electronic loads and reduce source current magnitude. This reduction in source current will help to reduce losses in cable and distribution transformer, which ultimately improve reliability and life-time of whole distribution system.

In case of unbalanced load condition, the UPF theory tried to equalise the current in all the phases and achieved it up to a satisfactory level. In case of distortion in load side, this theory has been successfully compensated the distortion well below the IEEE-519 standard limits, i.e., 5% of $THD_v$. However, in case of distortion coming from source side, the UPF theory failed to correct it. It is due to the fact that UPF sees the problems occurring after the PCC and correct them, but it does not notice the problems related to source side and as a result replicate problem of source in the reference current.

Based on this discussion, it can be concluded that UPF control algorithm is able to provide UPF in any abnormal condition both from source and or load side by compensating reactive power requirements from load. This can reduce the unbalanced load effects at PCC. It also minimises the harmonic distortion if harmonics are generated from load side only.

## References

Abellan, A., Benavent, J.M., Garcera, G. and Cerver, D. (2002) 'Fixed frequency current controller applied to shunt active filters with UPF control in four-wire power systems', Paper presented at the *IECON 2002 – IEEE 2002 28th Annual Conference of the Industrial Electronics Society.*

Akagi, H. (2005) 'Active harmonic filters', *Proceedings of the IEEE*, Vol. 93, No. 12, pp.2128–2141.

Alam, M.J.E., Muttaqi, K.M. and Sutanto, D. (2015) 'Alleviation of neutral-to-ground potential rise under unbalanced allocation of rooftop PV using distributed energy storage', *IEEE Transactions on Sustainable Energy*, Vol. 6, No. 3, pp.889–898.

Albatran, S., Koran, A., Smadi, I.A. and Ahmad, H.J. (2018) 'Optimal design of passive RC-damped LCL filter for grid-connected voltage source inverters', *Electrical Engineering*, Vol. 100, No. 4, pp.2499–2508.

Aleem, S.H.A. and Zobaa, A.F. (2017) 'Optimal C-type filter for harmonics mitigation and resonance damping in industrial distribution systems', *Electrical Engineering*, Vol. 99, No. 1, pp.107–118.

Asiminoaei, L., Wiechowski, W., Blaabjerg, F., Krzeszowiak, T. and Kedra, B. (2006) 'A new control structure for hybrid power filter to reduce the inverter power rating', Paper presented at the *IECON 2006 – 32nd Annual Conference on IEEE Industrial Electronics*.

Bangarraju, J., Rajagopal, V. and Jayalaxmi, A. (2014) 'Unit template synchronous reference frame theory based control algorithm for DSTATCOM', *Journal of the Institution of Engineers (India): Series B*, Vol. 95, No. 2, pp.135–141, DOI: 10.1007/s40031-014-0087-y.

Benysek, G. and Pasko, M. (2012) *Power Theories for Improved Power Quality*, Springer, London.

Bose, B.K. (2009) 'Power electronics and motor drives recent progress and perspective', *IEEE Transactions on Industrial Electronics*, Vol. 56, No. 2, pp.581–588.

Brito, M.E.C., Cavalcanti, M.C., Limongi, L.R., Neves, F.A.S. and Azevedo, G.M.S. (2018) 'Adjustable VAr compensator with losses reduction in the electric system', *Electrical Engineering*, Vol. 100, No. 4, pp.2165–2175, DOI: 10.1007/s00202-018-0692-x.

Chapman, D. (2001) 'Harmonics causes and effects', in *Power Quality Application Guide*, European Copper Institute and Leonardo ENERGY.

Chen, L. and von Jouanne, A. (2001) 'A comparison and assessment of hybrid filter topologies and control algorithms', Paper presented at the *2001 IEEE 32nd Annual Power Electronics Specialists Conference*, PESC.

Council of European Energy Regulators (CEER) (2011) *5th CEER Benchmarking Report on the Quality of Electricity Supply*.

Das, J. (2003) 'Passive filters-potentialities and limitations', Paper presented at the *Conference Record of the 2003 Annual Pulp and Paper Industry Technical Conference, 2003*.

Elhaj, N., Djeghloud, H., Sedra, M.B. and Jarou, T. (2018) 'A comparative analysis of DFPI correctors and different techniques to regulate a shunt active power filter', *International Journal of Power Electronics*, Vol. 9, No. 1, pp.79–98.

Elphick, S., Ciufo, P., Drury, G., Smith, V., Perera, S. and Gosbell, V. (2017) 'Large scale proactive power-quality monitoring: an example from Australia', *IEEE Transactions on Power Delivery*, Vol. 32, No. 2, pp.881–889.

Garg, R., Mahajan, P., Kumar, P. and Goel, R. (2014) 'Design of unity power factor controller for three-phase induction motor drive fed from single phase supply', *Journal of Automation and Control Engineering*, Vol. 2, No. 3, pp.221–227.

George, V. and Mishra, M.K. (2010) 'DSTATCOM topologies for three-phase high power applications', *International Journal of Power Electronics*, Vol. 2, No. 2, pp.107–124.

Gupta, N., Dubey, S.P. and Singh, S.P. (2011) 'Neural network-based shunt active filter with direct current control for power quality conditioning', *International Journal of Power Electronics*, Vol. 3, No. 6, pp.597–620.

Han, Y., Xu, L., Khan, M.M., Yao, G., Zhou, L-D. and Chen, C. (2010) 'Study on a novel approach to active power filter control using neural network-based harmonic identification scheme', *Electrical Engineering*, Vol. 91, No. 6, p.313, DOI: 10.1007/s00202-009-0143-9.

Iyer, S., Ghosh, A. and Joshi, A. (2005) 'Inverter topologies for DSTATCOM applications – a simulation study', *Electric Power Systems Research*, Vol. 75, Nos. 2–3, pp.161–170, DOI: 10.1016/j.epsr.2005.02.003.

Krismanto, A.U., Lomi, A. and Hartungi, R. (2012) 'Artificial neural network-based harmonics extraction algorithm for shunt active power filter control', *International Journal of Power Electronics*, Vol. 4, No. 3, pp.273–289.

Kumar, B.K., Mishra, M.K., Bhaskar, K.S. and Vardhana, P.H. (2008) 'PSO-based feedback controller design of DSTATCOM for load compensation with non-stiff sources', *International Journal of Power Electronics*, Vol. 1, No. 2, pp.191–205, DOI: 10.1504/IJPElec.2008.02235.

Kumar, D. and Zare, F. (2014) 'Analysis of harmonic mitigations using hybrid passive filters', Paper presented at the *2014 16th International Power Electronics and Motion Control Conference and Exposition*, 21–24 September.

Kumar, D. and Zare, F. (2016) 'Harmonic analysis of grid connected power electronic systems in low voltage distribution networks', *IEEE Journal of Emerging and Selected Topics in Power Electronics*, Vol. 4, No. 1, pp.70–79, DOI: 10.1109/JESTPE.2015.2454537.

Kumar, D., Davari, P., Zare, F. and Blaabjerg, F. (2017) 'Analysis of three-phase rectifier systems with controlled DC-link current under unbalanced grids', Paper presented at the *2017 IEEE Applied Power Electronics Conference and Exposition (APEC)*.

Leite, J.C., Abril, I.P., de Lima Tostes, M.E. and De Oliveira, R.C.L. (2017) 'Multi-objective optimization of passive filters in industrial power systems', *Electrical Engineering*, Vol. 99, No. 1, pp.387–395.

Litrán, S.P., Salmerón, P., Vázquez, J.R. and Flores, J.L. (2005) 'Compensation of voltage unbalance and current harmonics with a series active power filter', *Renewable Energy and Power Quality Journal*, Vol. 1, No. 3, pp.222–227.

Mahela, O.P. and Shaik, A.G. (2015) 'A review of distribution static compensator', *Renewable and Sustainable Energy Reviews*, Vol. 50, pp.531–546, DOI: 10.1016/j.rser.2015.05.018.

Menti, A., Zacharias, T. and Milias-Argitis, J. (2009) 'Optimal sizing and limitations of passive filters in the presence of background harmonic distortion', *Electrical Engineering*, Vol. 91, No. 2, pp.89–100.

Meral, M.E. and Çelik, D. (2018) 'Benchmarking simulation and theory of various PLLs produce orthogonal signals under abnormal electric grid conditions', *Electrical Engineering*, Vol. 100, No. 3, pp.1805–1817, DOI: 10.1007/s00202-017-0660-x.

Orts-Grau, S., Gimeno-Sales, F.J., Segui-Chilet, S., AbellÁn-GarcÍa, A., Alcaniz, M. and Masot-Peris, R. (2008) 'Selective shunt active power compensator applied in four-wire electrical systems based on IEEE Std. 1459', *IEEE Transactions on Power Delivery*, Vol. 23, No. 4, pp.2563–2574, DOI: 10.1109/TPWRD.2008.923414.

Rahmani, S., Hamadi, A., Mendalek, N. and Al-Haddad, K. (2009) 'A new control technique for three-phase shunt hybrid power filter', *IEEE Transactions on Industrial Electronics*, Vol. 56, No. 8, pp.2904–2915.

Rohilla, Y. and Pal, Y. (2013) 'T-connected transformer integrated three-leg VSC based 3P4W DSTATCOM for power quality improvement', Paper presented at the *2013 Nirma University International Conference on Engineering (NUiCONE)*, 28–30 November.

Saralaya, S. and Sharma, K.M. (2018) 'An improved control strategy without current sensors for DSTATCOM', *International Journal of Power Electronics*, Vol. 9, No. 2, pp.214–228.

Singh, B., Al-Haddad, K. and Chandra, A. (1999) 'A review of active filters for power quality improvement', *IEEE Transactions on Industrial Electronics*, Vol. 46, No. 5, pp.960–971.

Srikanthan, S. and Mishra, M.K. (2009) 'Ramp based constant frequency current control for DSTATCOM', *International Journal of Power Electronics*, Vol. 1, No. 3, pp.249–266, DOI: 10.1504/IJPElec.2009.023621.

Von Jouanne, A. and Banerjee, B. (2001) 'Assessment of voltage unbalance', *IEEE Transactions on Power Delivery*, Vol. 16, No. 4, pp.782–790.

Zare, F. and Kumar, D. (2016) 'Harmonics analysis of industrial and commercial distribution networks with high penetration of power electronics converters', Paper presented at the *2016 Australasian Universities Power Engineering Conference (AUPEC)*.

Zare, F., Soltani, H., Kumar, D., Davari, P., Delpino, H.A.M. and Blaabjerg, F. (2017) 'Harmonic emissions of three-phase diode rectifiers in distribution networks', *IEEE Access*, Vol. 5, pp.2819–2833, DOI: 10.1109/ACCESS.2017.2669578.